VERTICALLY ALIGNED CARBON NANOTUBES AS A FRAMEWORK FOR

MICROFABRICATION OF HIGH ASPECT RATIO MEMS

by

David Neil Hutchison

A senior thesis submitted to the faculty of

Brigham Young University

in partial fulfillment of the requirements for the degree of

Bachelor of Science

Department of Physics and Astronomy

Brigham Young University

August 2008

BRIGHAM YOUNG UNIVERSITY

DEPARTMENT APPROVAL

of a senior thesis submitted by

David Neil Hutchison

This thesis has been reviewed by the research advisor, research coordinator, and department chair and has been found to be satisfactory.

_____	_____
Date	Robert C. Davis, Advisor
_____	_____
Date	Eric Hintz, Research Coordinator
_____	_____
Date	Ross Spencer, Chair

ABSTRACT

VERTICALLY ALIGNED CARBON NANOTUBES AS A FRAMEWORK FOR

MICROFABRICATION OF HIGH ASPECT RATIO MEMS

David Neil Hutchison

Department of Physics and Astronomy

Bachelor of Science

We present a new technique using carbon nanotubes as a framework to make high aspect ratio structures from a variety of materials, and demonstrate its applicability to microelectromechanical systems. First, a "forest" of vertically-aligned carbon nanotubes (CNTs) is grown from a patterned catalyst film by chemical vapor deposition (CVD). Next, the spaces between CNTs are filled with silicon, silicon nitride, or other materials by CVD. Finally, parts of the structure may be released by a short reactive ion etch to expose an underlying sacrificial layer, followed by a wet etch of the sacrificial layer. In this way, structures as tall as 1 mm with minimum feature size of less than 3 μm (dependent on design geometry) can be fabricated from a wide variety of materials.

ACKNOWLEDGMENTS

Contents

List of Figures

Chapter 1

Introduction

1.1 Carbon nanotubes

The interest in carbon nanotubes (CNTs) and their applications in nanoscale engineering and electronics has been extraordinary in the last decade. CNTs are tubes of graphite usually grown from iron nanoparticles [1] or iron films [2]. They have diameters ranging from less than 1 nm to tens of nanometers, lengths up to about 1 cm, and can be single-walled or multi-walled (SWNTs or MWNTs, respectively) [3]. CNTs have many remarkable characteristics, including the highest tensile strength and elastic modulus of any material on earth. They can be either metallic or semiconducting, based on chirality [3]. The difficulty of manipulating individual nanotubes has led to interest in bulk nanotube materials such as vertically-aligned carbon nanotubes (CNTs). These so-called CNT "forests" are usually grown from an iron film that, upon annealing, produces catalyst particles with sufficient density that the tubes grow more or less vertically upward, held together by van der Waals forces [4]. CNT forests have attracted considerable interest for their excellent field emission characteristics [5, 6] and high surface area-to-volume ratio [7]. In this thesis I will examine

their potential as a three-dimensional framework for microfabrication of high aspect ratio structures, focusing especially on the application of these structures to micro-electromechanical systems (MEMS).

1.2 MEMS and DRIE

MEMS are tiny mechanical devices such as cantilevers and linear motors with dimensions on the scale of micrometers. They have been used in such devices as accelerometers, pressure sensors, inkjet printer heads, and gas sensors [8]. Often when making MEMS, a high aspect ratio is desirable or necessary for mechanical resilience and to keep the motion of the device in-plane. High aspect ratios also increase the surface area for capacitive MEMS (e.g. comb drives). Deep Reactive Ion Etching (DRIE) is the leading technique for fabricating high aspect ratio structures in current MEMS technology. However, DRIE is slow, difficult, expensive, and specific to silicon. Other similar deep etching processes have been found for other materials (e.g. titanium), but each new DRIE-like process invented is specific to a certain substrate. For these reasons, a new approach to microfabricating high aspect ratio structures is needed. In this thesis I present such an approach that may be used as an alternative to DRIE. This approach may also be cheaper and more scalable than DRIE, and it is more versatile since it can produce MEMS in a variety of materials.

It is important to note that vertically-aligned CNTs (hereafter referred to simply as "CNTs" or CNT forests) have been used before to make electromechanical switches [9–11], a type of MEMS device. However, as-grown carbon nanotubes are fragile and will tear off the surface with a puff of air or at the slightest touch of tweezers, so CNT forests may not be suitable for some MEMS devices. By contrast, we use the nanotubes to simply define the three-dimensional shape of the device which is then

filled with a filler material. We show that the resulting composite is much stronger than an unfilled forest, making it a more attractive option for MEMS.

1.3 CNT framework

To make high aspect ratio structures using a CNT framework, first vertically-aligned CNTs must be grown from a patterned catalyst film. The tubes are then coated with silicon or other materials by low-pressure chemical vapor deposition (LPCVD). The coating process fills the interstices between tubes but preserves the larger overall CNT pattern. Next, the moving parts of the structure are released by partial removal of the underlying SiO_2 sacrificial layer by a wet etch.

In this process, smaller features or those with etch holes in them are completely released, while the oxide layer under larger "anchor regions" is not completely removed and these areas remain attached to the substrate. In this way, parts of the MEMS structure can be made free to move while other parts remain anchored to the substrate. This release method was chosen for simplicity since it involves a one-step lithography process with no alignment, but for future, more complicated devices it may be advantageous to define anchor regions first, then align the MEMS pattern to the anchored regions using a multi-step lithography process.

Fig. 1.1 shows some high aspect-ratio devices fabricated in this process. Depending on the type of pattern being made (see Sec. 2.3.2), this CNT framework approach to microfabrication can result in feature sizes of less than 3 μm and vertical heights of up to 1 mm, compatible with most present industrial DRIE requirements. This technique only uses equipment commonly found in semiconductor fabrication laboratories, and hence is highly compatible with established fabrication processes.
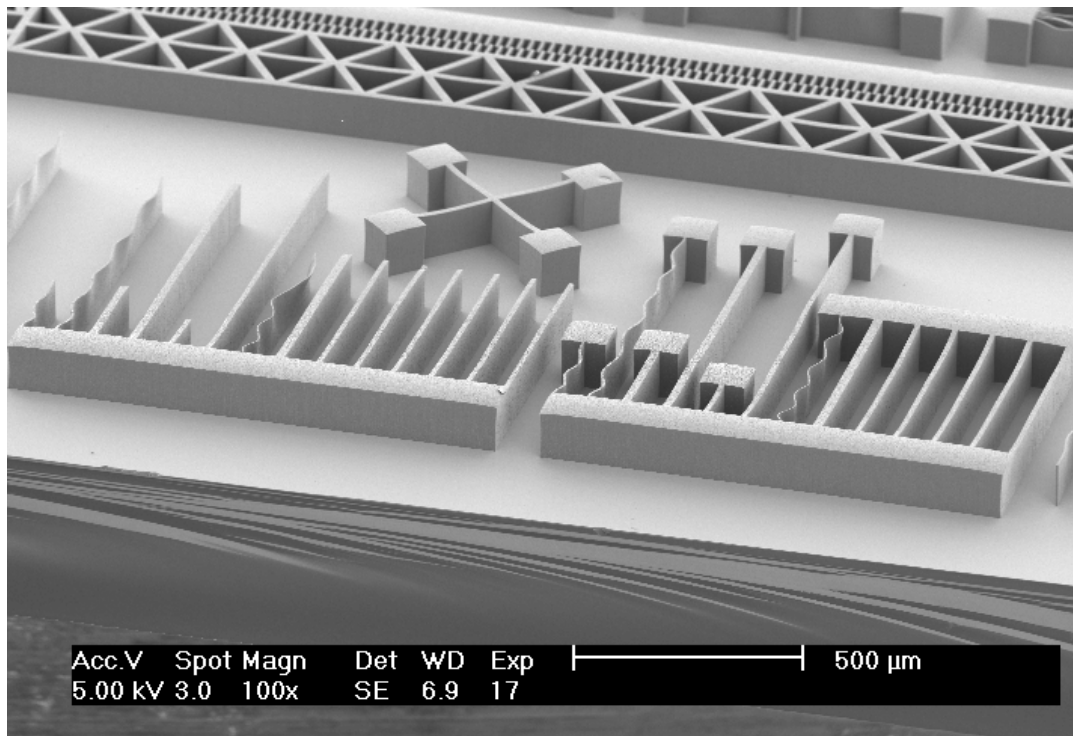
Figure 1.1 An SEM image of some high aspect ratio devices fabricated by filling a nanotube forest with silicon. (The devices in this image have not yet had the floor layer or sacrificial oxide layer removed.) In Sec. 2.3.1 I will address how to reduce the waviness problem exhibited by the thinnest cantilevers in the foreground. In the background is part of a comb drive, and the 'X' shaped structure is a Van Der Pauw device. This image was taken at 50° tilt.

Chapter 2

Methods and Results

2.1 Overview of Fabrication Procedure

In the CNT framework technique we developed, vertically-aligned carbon nanotubes (CNTs) are grown as a patterned forest. The space between tubes is then filled with silicon, silicon nitride, or other materials by low-pressure chemical vapor deposition (LPCVD). This deposition step coats each tube conformally until the entire structure is filled with the filler material, but preserves the overall micron-scale features of the pattern. The LPCVD deposition also deposits a thin "floor layer" on the substrate where there was no nanotube growth. Next, the floor layer must be removed with a short reactive ion etch to access the underlying SiO_2 sacrificial layer. Finally, parts of the structure are released by a etching the underlying sacrificial layer. The process is depicted in Fig. 2.1.
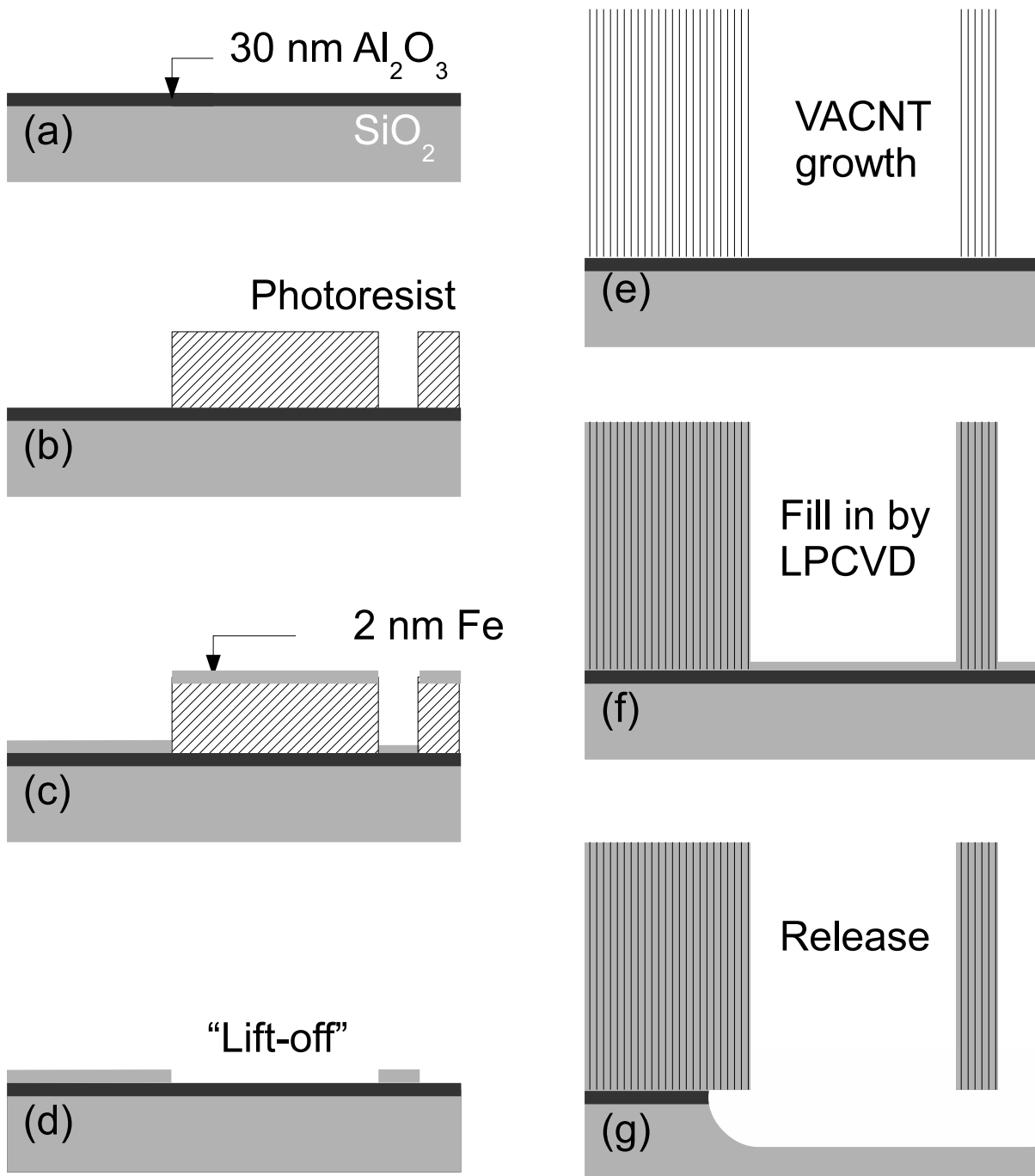
Figure 2.1 Process diagram. **(a)** 30 nm of alumina is evaporated by electron-beam evaporation on SiO$_2$. **(b)** AZ3330 photoresist is spun and patterned. **(c)** 7 nm of Fe is thermally evaporated on top of the photoresist. **(d)** The photoresist is lifted off in a resist stripper. **(e)** A forest of vertically-aligned carbon nanotubes is grown from the patterned iron film by chemical vapor deposition at 750 °C using C$_2$H$_4$ and H$_2$ feedstock gases. **(f)** Tubes are coated with Si or other materials by low-pressure chemical vapor deposition. **(g)** The underlying SiO$_2$ is etched to release parts of the structure.

2.2   Substrate Preparation

2.2.1   Methods

Beginning with a Si, SiO$_2$, or Si$_3$N$_4$ wafer, 30 nm of alumina (Al$_2$O$_3$) is deposited by electron-beam evaporation onto the substrate at a pressure of 30 μTorr or lower. We chose to begin with wafers having a 3 μm thick SiO$_2$ layer that would serve as a sacrificial layer later in the process, but we verified that CNTs grow equally well on silicon or silicon nitride wafers, as long as the alumina layer was present. The alumina appears to act as a diffusion barrier to reduce the amount of iron that is lost by diffusion into the substrate. It may also mediate the surface mobility of Fe as it is heated and thereby impact catalyst particle formation.

AZ3330 photoresist is then spun onto the sample to a thickness of about 1 μm, exposed in the desired pattern, and developed. Note that the developer etches alumina so the developing process (35 seconds in AZ 300 MIF developer) results in a reduction in the alumina thickness of about 3 nm at the places where the resist is developed, while the alumina that is under photoresist that does not develop remains the original thickness. This is important to know when trying to measure the thickness of the patterned Fe film by profilometer, since the measured Fe thickness with alumina present will be less than the actual Fe thickness due to the alumina etching in the photoresist developer.

Next, 4 nm of iron is deposited by thermal evaporation at a pressure of 4 μTorr or lower. The sample is then immersed in a resist stripper (Microposit 1165, MicroChem) and sonicated for 15 minutes. Following this "lift-off" step, the sample is removed from the stripper, and before the stripper residue dries it is quickly squirted with acetone for 1 minute, then with isopropanol for 1 minute, then blown dry with nitrogen gas.

Effect of Alumina Thickness

To test the effect of alumina thickness, a single Si wafer was coated with different thicknesses of alumina from 0.8 to 71 nm, by shadow-masking 1 cm^2 regions and doing many alumina evaporations. Photoresist was then patterned on top and 4 nm of Fe was evaporated on top of the entire wafer. The photoresist was lifted off and the wafer divided into small chips which were grown for 5 minutes at the standard conditions.

Effect of Fe Thickness

To test the effect of iron thickness, 22 nm of alumina was deposited by electron-beam evaporation and then photoresist was patterned on top. The wafer was divided into chips and a set of chips were put into the thermal evaporator for Fe evaporation. Several Fe thicknesses were deposited on different samples in the same run, by incrementally opening the shutter. Nanotubes were then grown for 5 minutes at the standard conditions.

2.2.2 Results

Effect of Alumina Thickness

The results are shown in Fig. 2.2(a). The thickness of alumina appears to have little effect on the height of the forest as long as there are at least 20 nm of alumina present. Between about 4–20 nm the height of the resulting forest seems to decrease slightly, though it is hard to say conclusively from these data. Below an alumina thickness of about 4 nm, there is no vertically-aligned growth observed, just poor, unaligned growth.

Forest height has been observed to depend on several things including how recently

the tube was cleaned, exact annealing times, the particulars of how each sample was prepared, and so forth, which may account for the scatter in the data. Individual samples usually grow to a very uniform height, but there is sometimes variation from sample to sample. However, this nonuniformity seems to be more controllable when the tube is frequently cleaned. (The quartz tube used for nanotube growth may be cleaned by passing air through it, bringing the tube to 950 °C in about 10 minutes, and then letting the tube cool to 250 °C or below in about 15 minutes.)

Effect of Fe Thickness

The results are shown in Fig. 2.2(b). Even though there is significant difference in forest height from run to run (probably for similar reasons as the scatter in the alumina data), it does clearly show several important features. First, there is a cutoff thickness of iron below which no forest growth is observed, probably due to the small amount of iron diffusing into the underlying alumina as the furnace is heating up before nanotube growth begins. Just above the cutoff thickness, the forest grows very tall except not always reliably—for example, the sample indicated by the arrow in Fig. 2.2(b) only supported forest growth on half of its surface, while the other half of its surface had no growth. Above the cutoff thickness, the forest height decreases with increasing thickness of iron. This might be because thicker iron layers form larger catalyst particles upon annealing (heating to growth temperature), which form larger tubes with more walls. These larger tubes require more carbon atoms to grow a certain length than smaller diameter tubes. Even though some iron presumably still diffuses into the alumina, there is enough iron remaining when the ethylene is turned on to catalyze nanotube growth. The range of thicknesses from about 3-5 nm seem to yield the most uniform growth. For thicker iron layers, there is shorter and less uniform growth observed until about 20 nm, above which no forest growth

Effect of alumina thickness on forest height after 5 min growth (with 4nm of patterned iron)

Effect of iron thickness on forest height after 5 min growth (with 22nm unpatterned alumina underneath)

(a)
Alumina thickness (nm)

(b)
Fe thickness (nm)

Run 1
Run 2
Run 3
Run 4
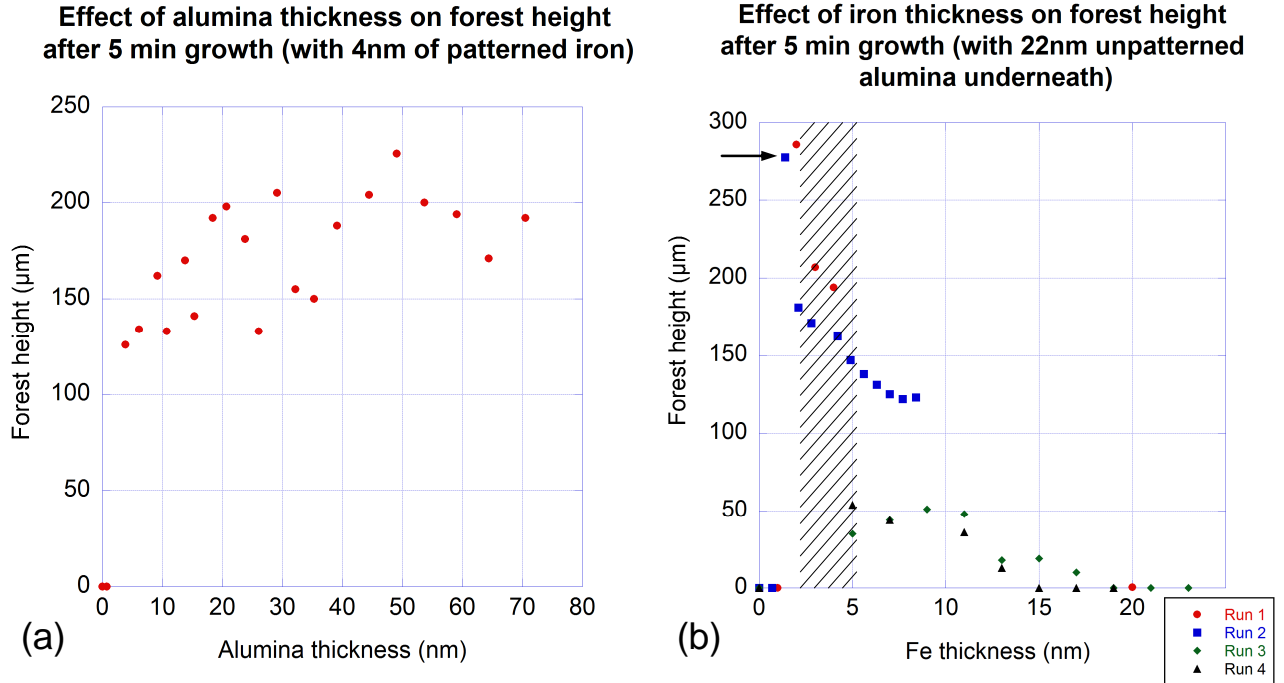
Figure 2.2 The effect on forest height of various thicknesses **(a)** for alumina, with 4 nm of iron on top, and **(b)** for iron, with 22 nm alumina underneath. The shaded region in (b) indicates the best range of iron thicknesses. Thinner or thicker iron films tend to grow non-uniform forests. The data point indicated by the arrow only grew on half of the substrate.

is observed. For such thick iron layers the iron may be unable to ball up during the annealing process and remains a film, preventing nanotube growth.

2.3 CNT Growth

2.3.1 Methods

The sample is placed on a quartz boat in a 1-inch quartz tube furnace (Lindberg Blue M EW-33850) and heated from room temperature to 750 °C flowing 500 sccm of H_2. The furnace reaches 750 °C in about 8 minutes, at which time the C_2H_4 flow is switched on to 700 sccm. If slower growth is desired, the gases may be diluted with argon. After the desired CNT length is obtained, the H_2 and C_2H_4 gases are
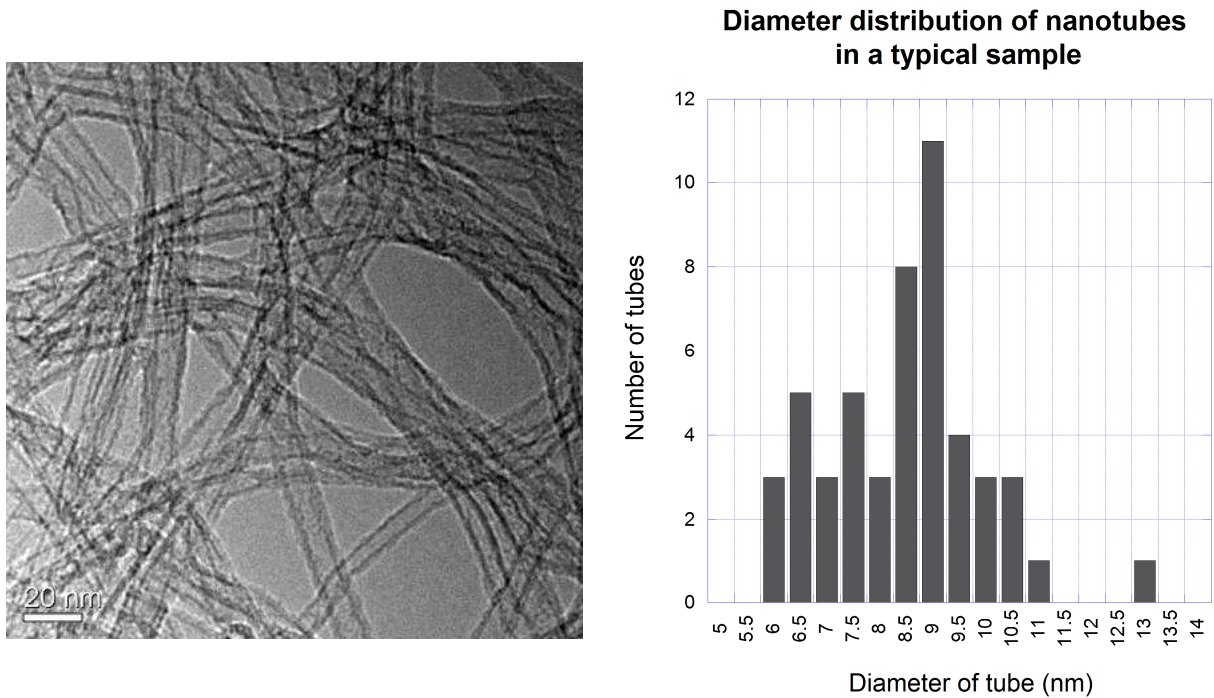
Figure 2.3 The diameter distribution of a sample of carbon nanotubes, measured by removing some tubes from the substrate and examining them with the transmission electron microscope.

turned off, Ar is turned on at 350 sccm and the furnace is cooled to 200 °C in about 5 minutes.

2.3.2 Results

Tube diameter

Our growth process was found to grow large, multi-walled nanotubes with an average diameter of 8.5 nm, as shown in Fig. 2.3. It is likely that this distribution will be different for different iron thicknesses but for the CNT framework technique, nanotubes of any diameter work (as long as they can grow tall, uniform forests). We sought to grow large, multi-walled nanotubes because they are known to grow much taller than small, single-walled nanotubes for the same growth conditions. [12]

Sidewall Roughness

The nanotubes do not grow up exactly parallel to each other, but rather in a wavy manner, resulting in something that looks like "steel wool" when viewed by SEM (Fig. 2.5(b)). This results in an intrinsic side-wall roughness in the final, coated nanotube structures, typically about 100-300 nm. This is similar to the side-wall roughness of holes made by deep reactive ion etching (DRIE), which can range from about 50-300nm.

Forest Bending

Thin forest walls, like those shown in Fig. 2.4(a) and (b), and Fig. 2.5(a) and (b), tend to bend over if grown much taller than their width. Most MEMS features can be made larger than that but when smaller features are desired this problem can be reduced by using what we call "self-supporting architectures." For example when designing thin, compliant members they may be periodically crossed at right angles with "crossbars" as shown in Fig. 2.5(c). This allows a thin forest wall to be grown much taller than possible without the crossbars, while maintaining high compliance. As an extreme example of self-supporting architectures, consider the difference between Fig. 2.4(b) and (c). The 3 μm lines in (b) cannot grow very tall without bending over, but if those lines are crossed at right angles with another array of 3 μm lines, the forest can grow as tall as nanotubes can grow without any sign of bending over or the holes closing off. Fig. 2.4(d) shows a top view of the forest in (c). We have been able to grow forests up to 1 mm tall in 30 minutes, after which time the nanotube growth seems to have essentially stopped.
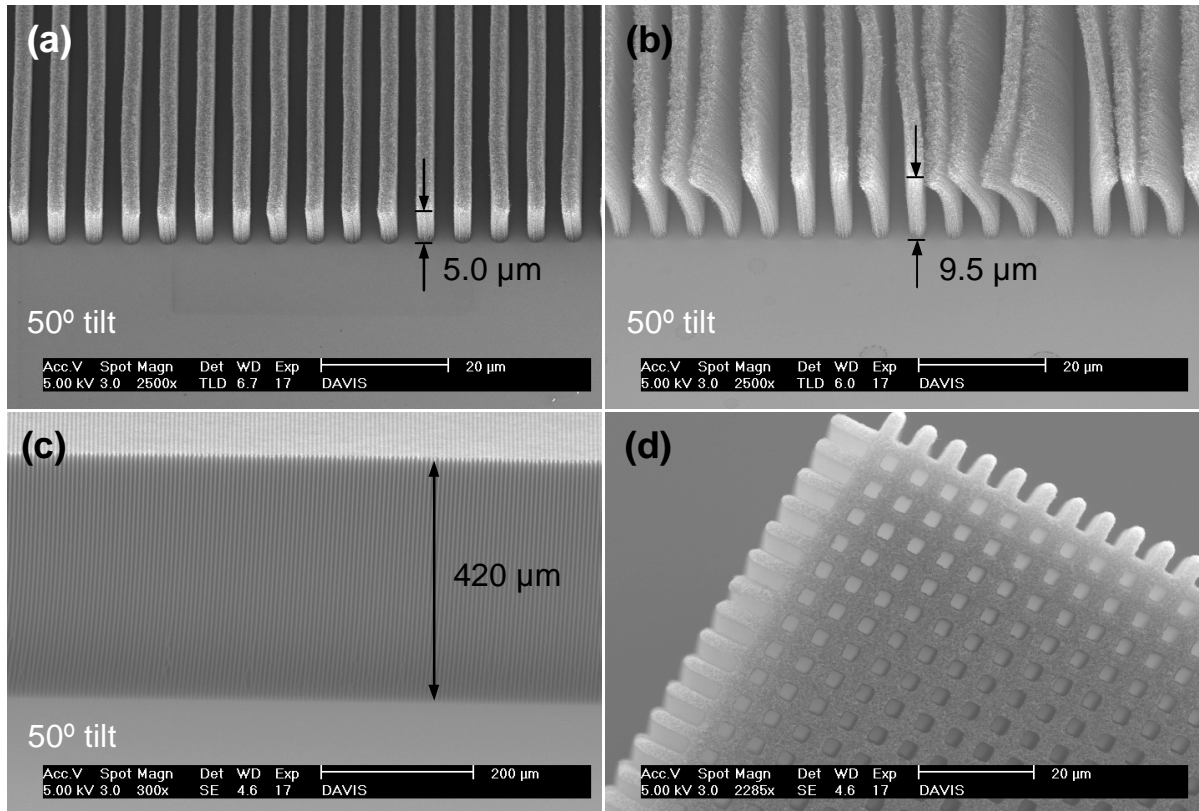
Figure 2.4 Reducing the effect of small features to bend over by mask design. **(a)** 3.0 μm forest "hedges" with 2.6 μm gaps between them. The forest lines do not bend over significantly when grown to a height of 5.0 μm. **(b)** If the same pattern is grown taller, it reaches a point where it no longer grows straight lines. **(c)** When the same line/space pattern is made into a grid pattern, there appears to be no limit to how tall the forest will be while still preserving the features (except for the limit imposed by how tall the forest can physically be grown—we have grown forests up to 1 mm tall). This image is a tilted image (50° tilt) showing the side of a 3 μm grid. The holes run down the entire height of this structure. **(d)** Top view of (c). (Note: Due to geometrical factors, vertical measurements in images that were taken at 50° tilt are actually 30% higher than they appear. Horizontal measurements are unchanged.) See Fig. 2.5 for more examples of reducing this effect by mask design.
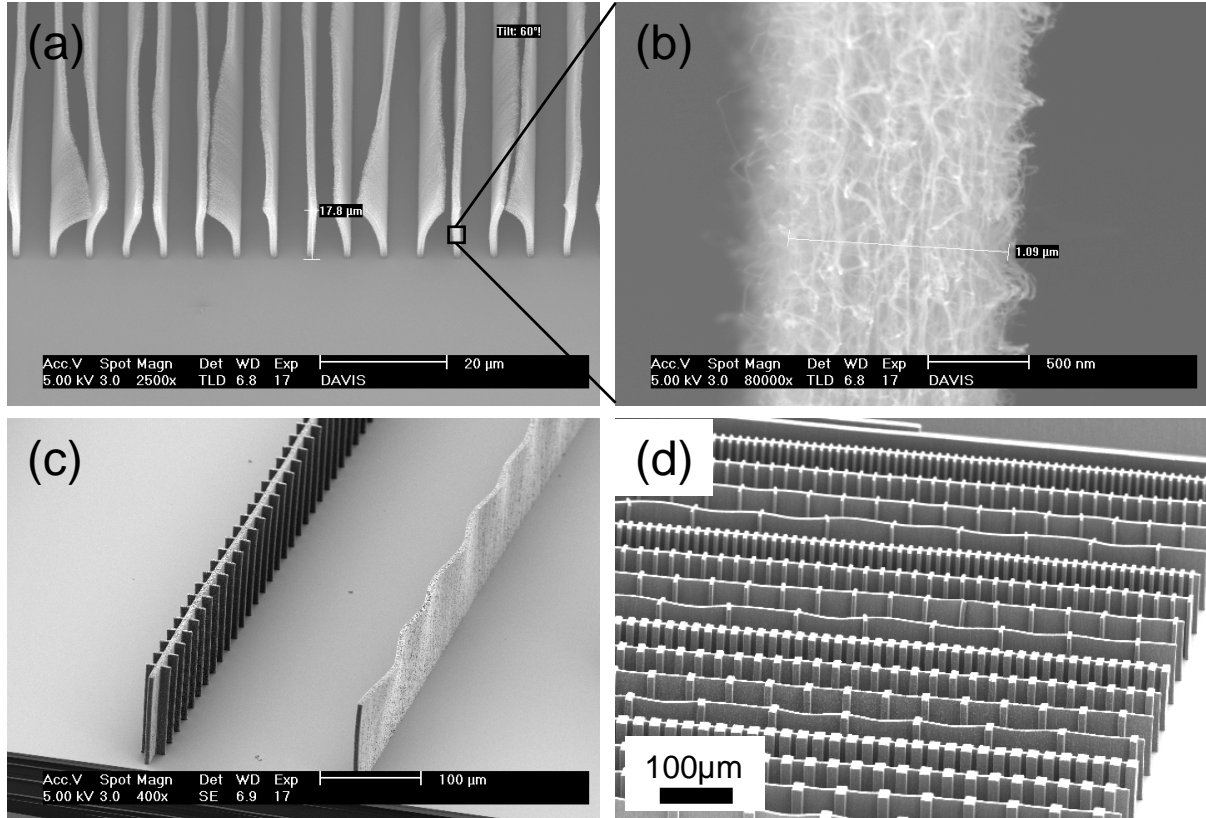
Figure 2.5 SEM images demonstrating as-grown sidewall roughness and demonstrating the usefulness of self-supporting geometries. **(a)** Lines of CNTs, 1 μm wide, before LPCVD coating showing how small features bend over if grown past a certain height for a given width of line. Image is at 50° tilt. **(b)** Higher magnification view of (a), showing typical sidewall roughness. Image is at 50° tilt. **(c)** Two lines, 5 μm wide, 100 μm tall, with crossbars (left) and no crossbars (right). Notice that the very thin forests of this width are not straight when grown to this height if grown as unsupported lines (however, for growths less than about 40 μm tall, the line on the right will grow straight too). Of course, a forest line may simply be grown wider in order to prevent it from bending over, but the essential point is that the crossbar architecture still allows the main line to be thin and highly compliant. Image is at 60° tilt. **(d)** The effect of crossbar spacing. For this particular height (100 μm), a 15 μm crossbar spacing seems to reliably provide straight lines. The width of the crossbars themselves seems to have no effect on the straightness of the lines.

2.4   As-Grown Forest Density

2.4.1   Methods

We would like to know how dense the nanotube framework is, so that after filling the interstices with a filler material we will know how much of the resulting structure is carbon, and how much is the filler material. To this end, squares of iron catalyst film 0.5 cm on a side were lithographically patterned and then the substrate was weighed on a microbalance with accuracy of 1 μg (Mettler UMT2). We then grew forests up to 0.7 mm tall from these substrates and weighed them again. We found the volume each forest occupies by measuring the height of the forest by clamping the sample edge-up and measuring the height of the sample with an optical microscope. The height was measured at several different places along the edge of the forest to ensure the forest was a uniform height. Knowing the volume and mass of nanotubes, the carbon density was calculated.

2.4.2   Results

As an initial measurement, the first forest was measured to be 30 μg on a scale with resolution of 10 μg, and its height measured to be 0.01 cm with an optical microscope. This gives a density of about 10 kg/m^3. Those measurements were not very accurate but gave us a ballpark idea of the density to expect. Next, two more solid blocks of vertically-aligned CNTs of the same size were grown, and weighed on a more accurate microbalance with accuracy of 0.1 μg. The height was measured with an optical microscope at each of the four corners of the forest, averaged, and the forest volume was computed. The two forests were found to have densities of 9.19 and 8.73 kg/m^3, or 8.96 kg/m^3 when averaged. This value is compared to some well-known low-density materials in Table 2.4.2.

Material	Density (kg/m^3)
Air	1.2
Silica aerogel: record low density [13]	1.9
Measured density of CNT forest	**9.0**
Silica aerogel: usual density range	10 - 500
Expanded polystyrene	25 - 200

Table 2.5.2 Densities for some low-density materials.

2.5 Filling with Polysilicon

2.5.1 Methods

The resulting patterned nanotube forests are then filled in by low-pressure chemical vapor deposition (LPCVD). This thesis will focus on our results of filling in the forest with undoped polycrystalline silicon, but we have also filled with other materials (see Sec. 2.6). To fill the forests with a conformal polycrystalline Si film, we used an LPCVD furnace (Canary stack furnace) at 200 mTorr and substrate temperature of 580 °C, flowing 20 sccm of SiH$_4$, for 2 hours 50 minutes, resulting in a deposition rate on a planar surface (or equivalently, a radial deposition rate on the carbon nanotubes) of 1.8 nm/min. The LPCVD tube is then vented with N$_2$ and the sample pulled out at a rate of about 1 cm/s.

2.5.2 Results

Vapor Access Holes

Very tall forests cannot be filled with this process unless vertical "vapor access holes" are made by inserting the desired hole geometries into the original photomask. Square

access holes of 3 μm across, spaced 3 μm apart, allow the polysilicon to fill the forest about to a depth about ten times greater than if the holes were not there (Fig. 2.6).

We varied the hole size and hole spacing to see the effect on how well the forest is filled. All forests studied in the remainder of this Methods section are the same height and were filled by undoped polysilicon in the same tube at the same time. For large square holes about 90 μm across (Fig. 2.7(a)) the forest is filled uniformly. For small holes about 3 μm across (2 μm after filling), the forest is still solid but the filling is not as uniform (Fig. 2.7(b)).

Notice that Fig. 2.7 (a) and (b) are both at the same magnification, so we can directly compare the two samples. The only thing that was varied was the size (and therefore spacing) of the holes. Patterns with large holes allow gas to enter the forest from many directions and fill more uniformly and completely than patterns with small holes.

We also studied the effect of hole spacing for a constant hole size (Fig. 2.8). Evidently, the forest is filled more solidly for more closely spaced holes.

The Floor Layer

The Si LPCVD filling step not only coats the nanotubes, it also deposits a layer of Si where there are no nanotubes (Fig. 2.9). This floor layer must be removed as described in Sec. 2.7 in order for the underlying sacrificial oxide layer to be removed.

TEM Studies of Polycrystalline Silicon Grains

The present recipe for depositing polysilicon seems to form grains of a wide range of shapes and sizes (up to about 100 nm across) within the forest (Fig. 2.10). When the forest becomes completely filled, if the polysilicon deposition is continued as shown
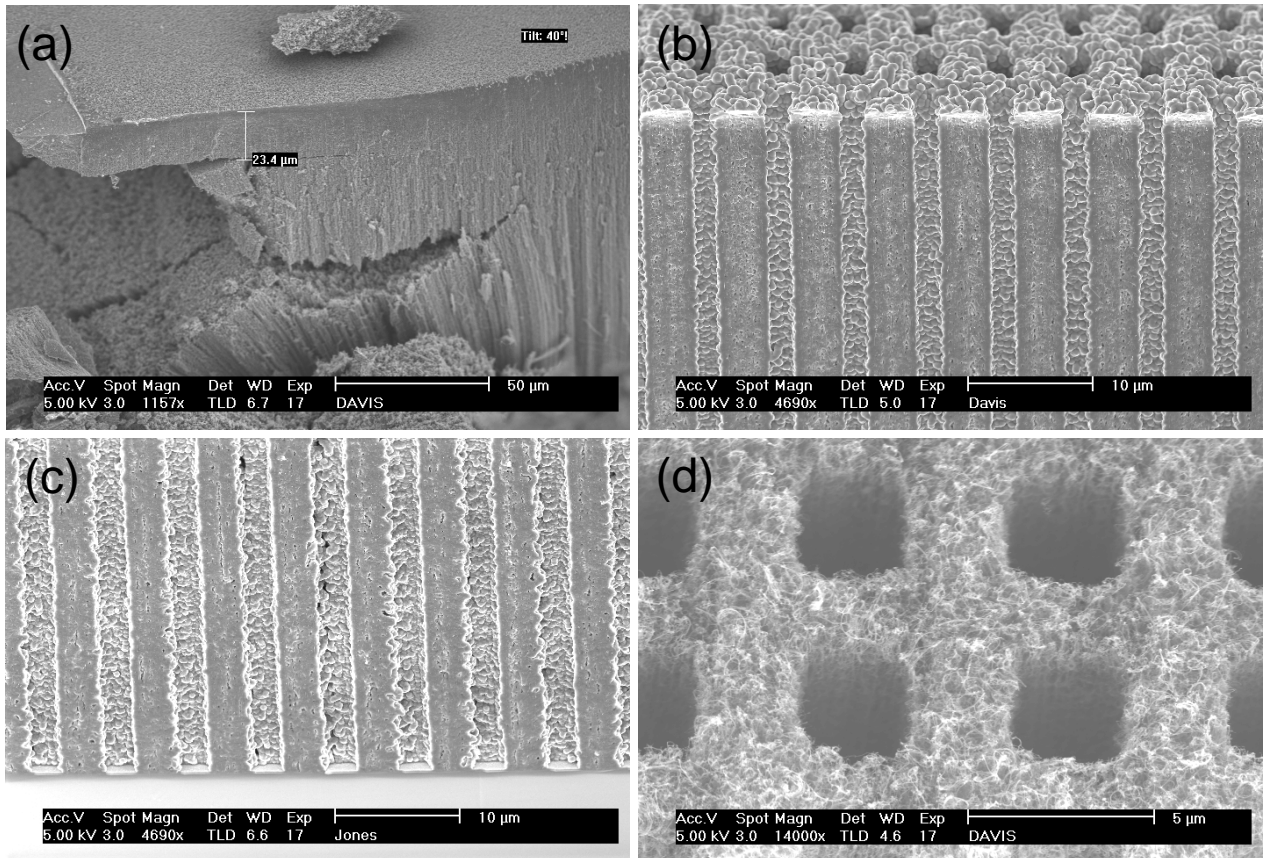
Figure 2.6 The effect of vapor access holes on filling very tall forests. **(a)** A cross-section of a 500 μm-tall filled forest without patterning, showing that it is only filled completely to a depth of about 20 μm. This image shows the forest after being broken open by tweezers and imaged at 50° tilt. Deeper than about 20 μm, the filling is only partial and the tubes have torn away. **(b),(c)** The top and bottom, respectively, of a 170 μm-tall forest with 3 μm holes spaced 3 μm apart. The forest is filled completely both at the top and bottom across the entire sample. These images show the filled forest after the whole Si substrate and nanotube composite were cleaved vertically, imaged at 50° tilt. **(d)** A top view of the forest in (b), before filling, showing the shape of the holes. Images (b), (c), and (d) are the same pattern as shown in Fig. 2.4 (c) and (d) after filling with silicon.

Hole   Forest   Hole

(a)

Acc.V	Spot	Magn	Det	WD	Exp		5 µm
5.00 kV	3.0	8787x	TLD	6.5	17	DAVIS	

Forest   Hole   Forest   Hole   Forest

(b)

Acc.V	Spot	Magn	Det	WD	Exp		5 µm
5.00 kV	3.0	8787x	TLD	6.5	17	DAVIS	
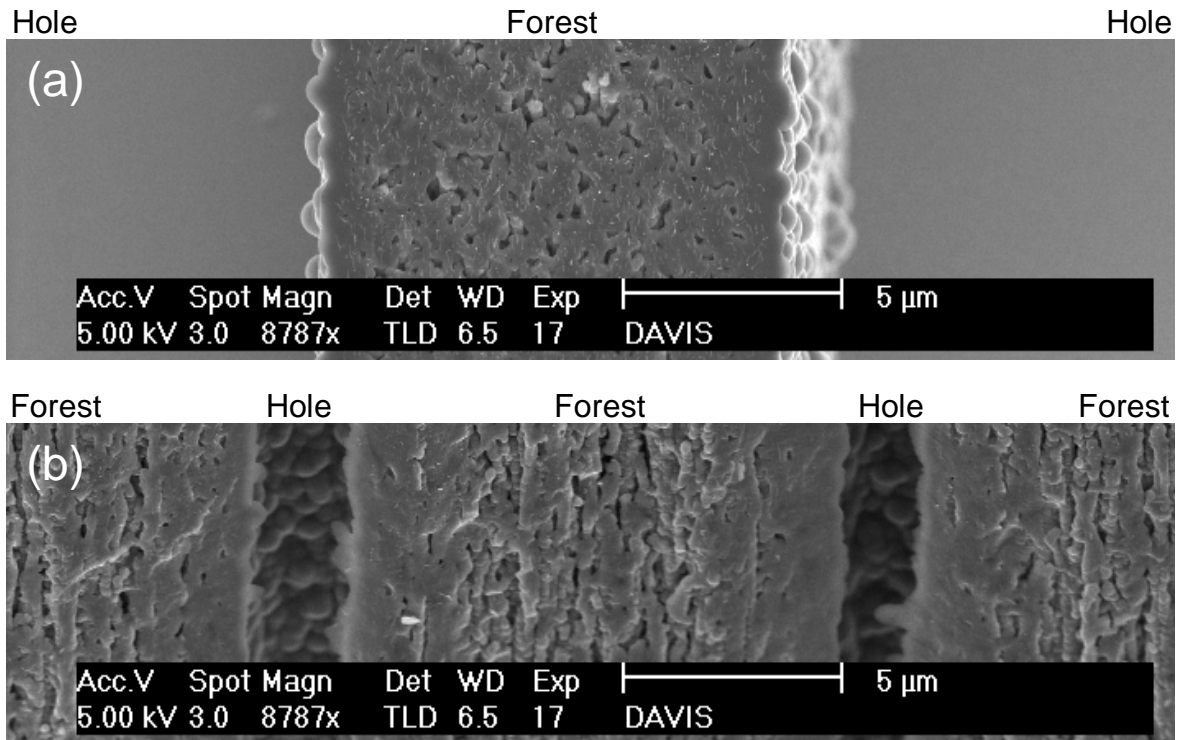
Figure 2.7 The effect of hole size on the filling of forests. These images show the filled forest after the whole Si substrate and nanotube composite were cleaved vertically, imaged at 50° tilt. **(a)** 90 µm holes. **(b)** 3 µm holes (which become 2 µm across after filling). The forest is filled more uniformly for large holes.

Hole   Hole

Forest   Forest   Forest
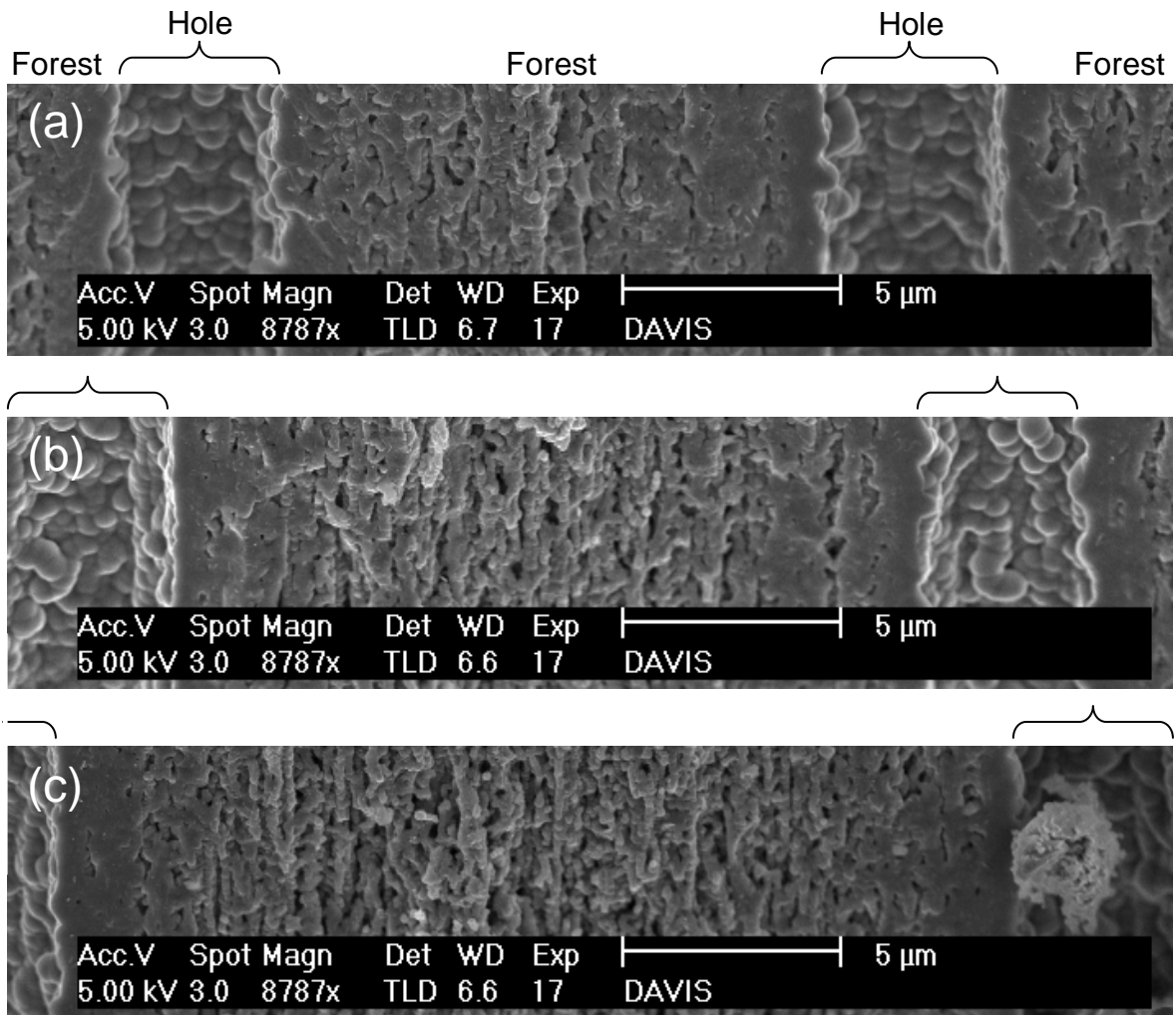
Figure 2.8 The effect of hole spacing on the filling of forests. These images show the filled forest after the whole Si substrate and nanotube composite were cleaved vertically, imaged at 50° tilt, all at the same magnification. The holes were all about 5 μm wide (4 μm after filling), spaced in a square grid different spacings apart: **(a)** 12 μm spacing, **(b)** 16 μm spacing **(c)** 21 μm spacing. The forest is filled more solidly for more closely spaced holes.
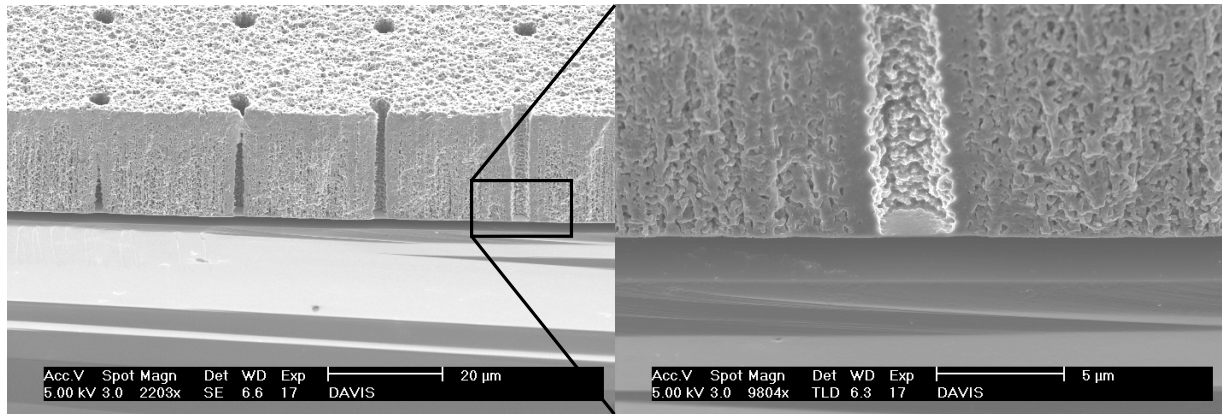
Figure 2.9 The "floor" layer. This forest was filled with Si, and put in the RIE for long enough to remove the floor where it needed to be removed. Next the sample was cleaved and put in BOE for long enough to release the moving parts of the MEMS on this structure. The previously-cleaved edge of the sample was then imaged by SEM at 50° tilt. Notice that the small 3 μm vapor access holes (which are closer to 2 μm in diameter after filling) were not big enough for the RIE to remove their floor layer. In this way, a tall forest can be filled but still remain anchored to the substrate. The right-hand image shows the floor layer at a higher magnification.

in Fig. 2.11, the polysilicon forms columnar grains growing perpendicularly from the substrate and perpendicularly from the forest.

Voids

Tubes are coated radially by the filler, which results in some small voids becoming shut off from further deposition. This results in a porous composite as shown in Fig. 2.12.
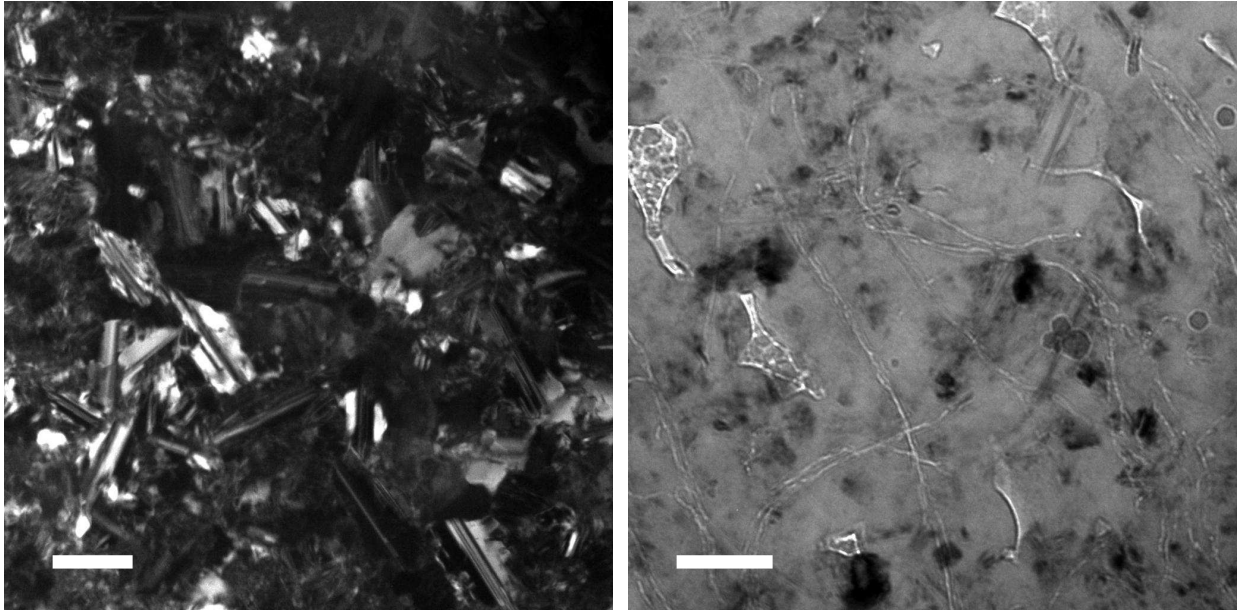
Figure 2.10 Transmission electron microscope (TEM) images of a polished vertical cross-section of a filled forest, showing the inter-tube silicon grains. **(a)** Dark-field image, scale bar 100 nm. **(b)** Bright-field image of a different part of the sample, scale bar 100 nm. The nanotubes are visible, embedded in the silicon filler. Some voids are also visible as lighter regions.
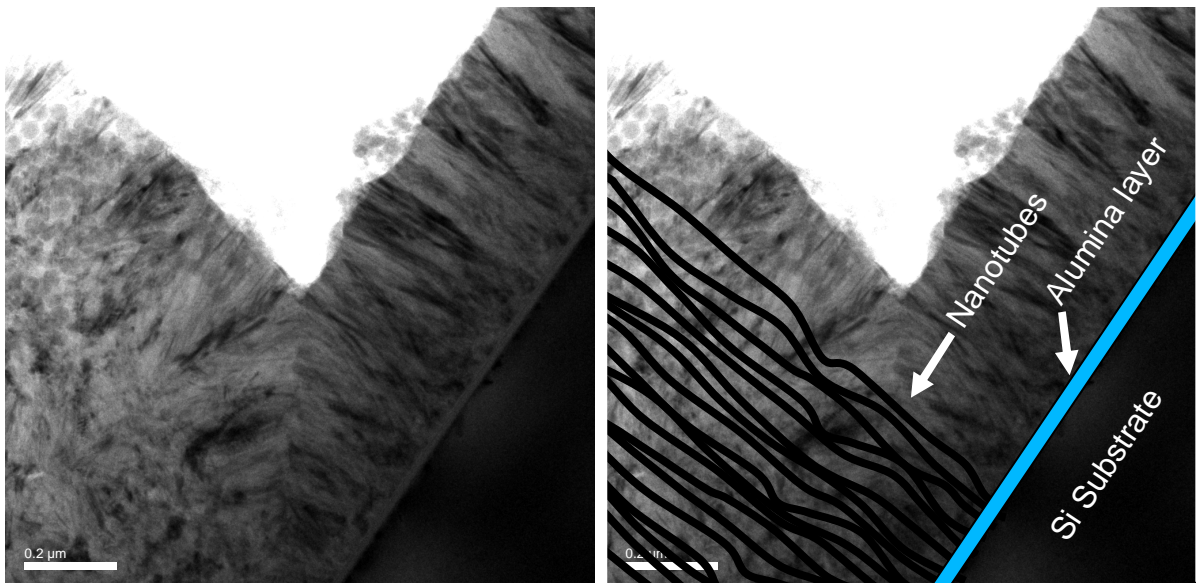
Figure 2.11 TEM images of a polished vertical cross-section of a filled forest. The inter-tube silicon grains are irregular in shape and the grains at the edge of the forest are columnar. **(a)** Bare TEM image, scale bar 0.2 μm. **(b)** The same image, overlaid with shapes to point out relevant features. The substrate is at bottom right, and the nanotubes are represented as wavy lines at bottom left.
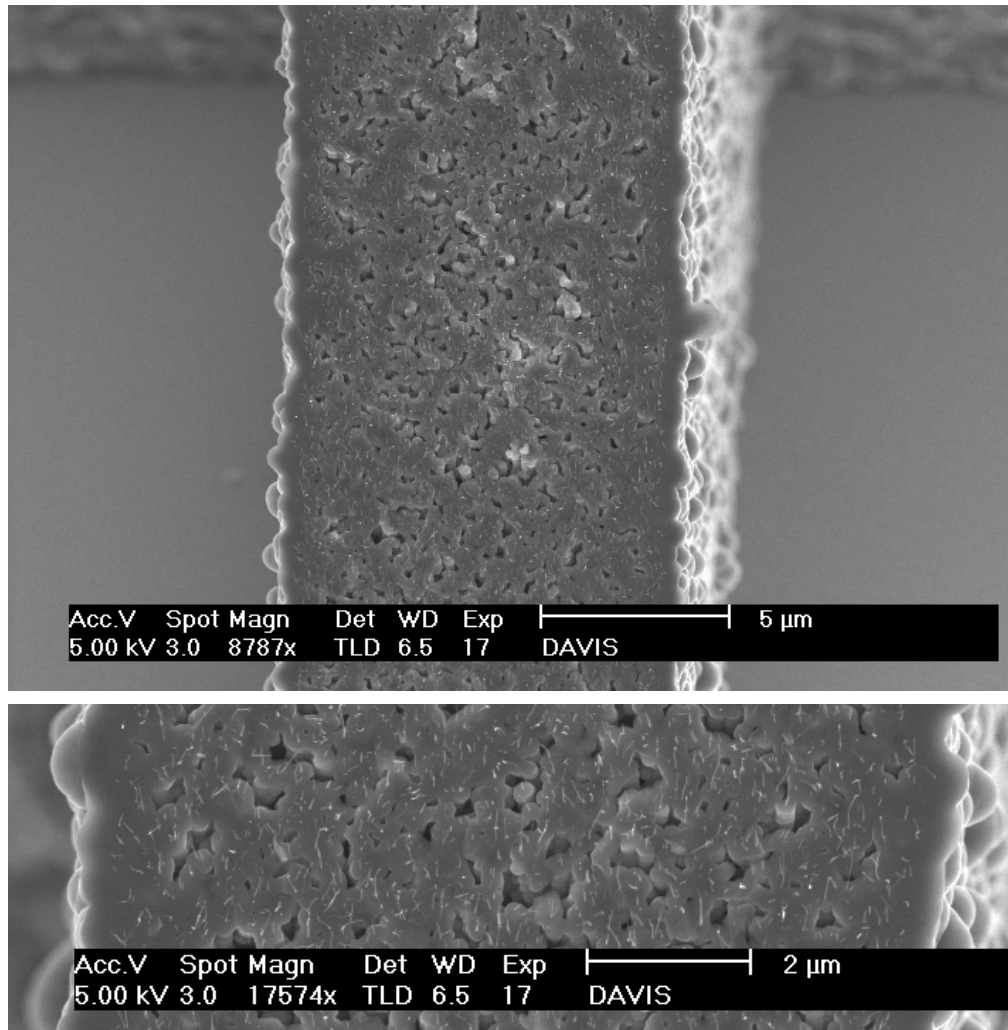
Figure 2.12 Voids in the composite. Small pockets or voids get shut off
from further deposition as each tube is coated radially. This is unavoidable
(no pun intended) unless perhaps the filler is something that is very mobile
while it is adsorbing to the nanotubes. This image shows a vertical cross-
section of part of a MEMS device. Notice the small tubes protruding from
the cleaved edge of the composite, particularly evident in the bottom (higher
magnification) image.

2.6   Filling With Other Materials

2.6.1   Significance

As shown in Fig. 2.13, most of the elements in the periodic table have been deposited by CVD, some in combinations (such as silicon nitride or polymers), but many in elemental form [14]. Most of our experiments to date have focused on filling with silicon, but it is possible to fill with other materials. This is significant because it may allow MEMS to be made from a wide variety of materials with a wide variety of material properties. Therefore, this fabrication technique may be useful for making MEMS that are resistant to high temperatures or harsh chemical environments, or out of materials that have traditionally been unavailable for MEMS because they are difficult to etch. It may allow MEMS engineers to tailor the working material to suit the application, such as filling a forest with a material with high thermal expansion coefficient in order to optimize thermomechanical sensors or actuators. This is perhaps the most compelling reason for continued development of the CNT framework technique.

Existing techniques for micromachining of high aspect ratio structures include the Bosch process for bulk micromachining of silicon [15], and the MARIO process for titanium [16], but each existing technique involves etching, and therefore is specific to a certain material. Of course, there will be carbon nanotubes embedded in the final structure but as shown in Sec. 2.4, the carbon volume fraction is only a few percent of the total volume, so the final structure consists mainly of the filler material with relatively little carbon.

Fillers that may be interesting to investigate include metals (especially those that are resistant to high temperatures like tungsten), polymers, and ceramics. As shown in Sec. 2.8, even insulating fillers may be used for conductive MEMS, since the nan-

1	2	3	4	5	6	7	8	9	10	11	12	13	14	15	16	17	18
1 H																	2 He
3 Li	4 Be											5 B	6 C	7 N	8 O	9 F	10 Ne
11 Na	12 Mg											13 Al	14 Si	15 P	16 S	17 Cl	18 Ar
19 K	20 Ca	21 Sc	22 Ti	23 V	24 Cr	25 Mn	26 Fe	27 Co	28 Ni	29 Cu	30 Zn	31 Ga	32 Ge	33 As	34 Se	35 Br	36 Kr
37 Rb	38 Sr	39 Y	40 Zr	41 Nb	42 Mo	43 Tc	44 Ru	45 Rh	46 Pd	47 Ag	48 Cd	49 In	50 Sn	51 Sb	52 Te	53 I	54 Xe
55 Cs	56 Ba	*	72 Hf	73 Ta	74 W	75 Re	76 Os	77 Ir	78 Pt	79 Au	80 Hg	81 Tl	82 Pb	83 Bi	84 Po	85 At	86 Rn
87 Fr	88 Ra	**	104 Rf	105 Db	106 Sg	107 Bh	108 Hs	109 Mt									

*	57 La	58 Ce	59 Pr	60 Nd	61 Pm	62 Sm	63 Eu	64 Gd	65 Tb	66 Dy	67 Ho	68 Er	69 Tm	70 Yb	71 Lu
**	89 Ac	90 Th	91 Pa	92 U	93 Np	94 Pu	95 Am	96 Cm	97 Bk	98 Cf	99 Es	100 Fm	101 Md	102 No	103 Lr

Figure 2.13 The periodic table, where shaded boxes indicate elements that have been deposited by CVD [14].

otubes provide an electrically conductive path through the composite.

2.6.2   Methods

To demonstrate that the nanotube framework technique is not limited to polysilicon, we have made a working bistable mechanism by filling a forest of nanotubes with silicon nitride and releasing the device. The silicon nitride was deposited at 720 °C and 200 mTorr in an LPCVD furnace (Canary stack furnace, using a different tube than the polysilicon process). The tube was evacuated and NH_3 flowed for 3 minutes at 14 sccm for a "pre-soak". Next the NH_3 was kept flowing and dichlorosilane was turned on at a flow rate of 10 sccm. After 3 hours, the dichlorosilane is turned off and NH_3 is allowed to continue flowing for 3 minutes to remove unreacted dichlorosilane. Finally the LPCVD tube is flushed and vented with N_2 and the sample pulled out at a rate of about 1 cm/s. This results in a nearly stoichiometric silicon nitride, evidenced by the index of refraction of a 200 nm film deposited on a planar Si substrate which
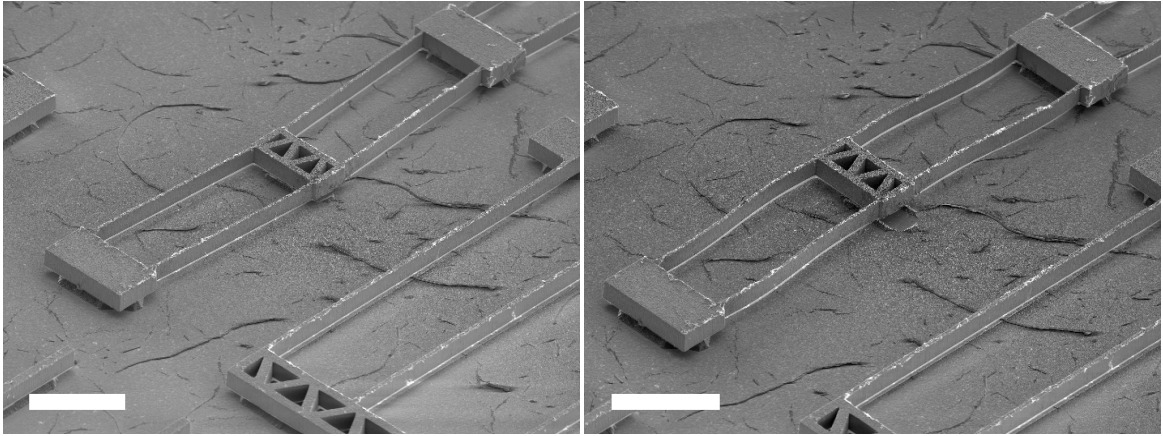
Figure 2.14 A bistable mechanism made by filling a nanotube forest with silicon nitride and then etching the underlying silicon with KOH. This demonstrates that this technique may be used to make high aspect ratio MEMS from materials other than silicon. The bistable mechanism is shown in **(a)** first position and **(b)** second position. Scale bars are both 200 μm. The dark lines underneath the device seem to result from the KOH etching process.

we measured by Filmetrics (Filmetrics F20, Model 205-01350) to be 1.9, compared with 2.0 for truly stoichiometric Si_3N_4.

These particular devices were not grown on a pre-deposited SiO_2 sacrificial layer, but instead grown on a Si wafer (with the necessary 30 nm alumina diffusion barrier layer). The underlying silicon was etched to release the devices in 45% KOH solution at 60 °C for 70 minutes.

We have also deposited combinations of fillers (such as 20 nm of polysilicon on a forest and then filled the rest of the forest with silicon nitride). We presume that combinations of fillers achieve continuously tunable material properties simply by varying continuously the thickness of each layer, but as yet we have not tested the mechanical properties of combinations of fillers.

We have also filled with amorphous carbon by heating the sample after nanotube growth from the growth temperature to 950 °C in C_2H_4, and allowing carbon to deposit for 20 minutes after reaching 950 °C.
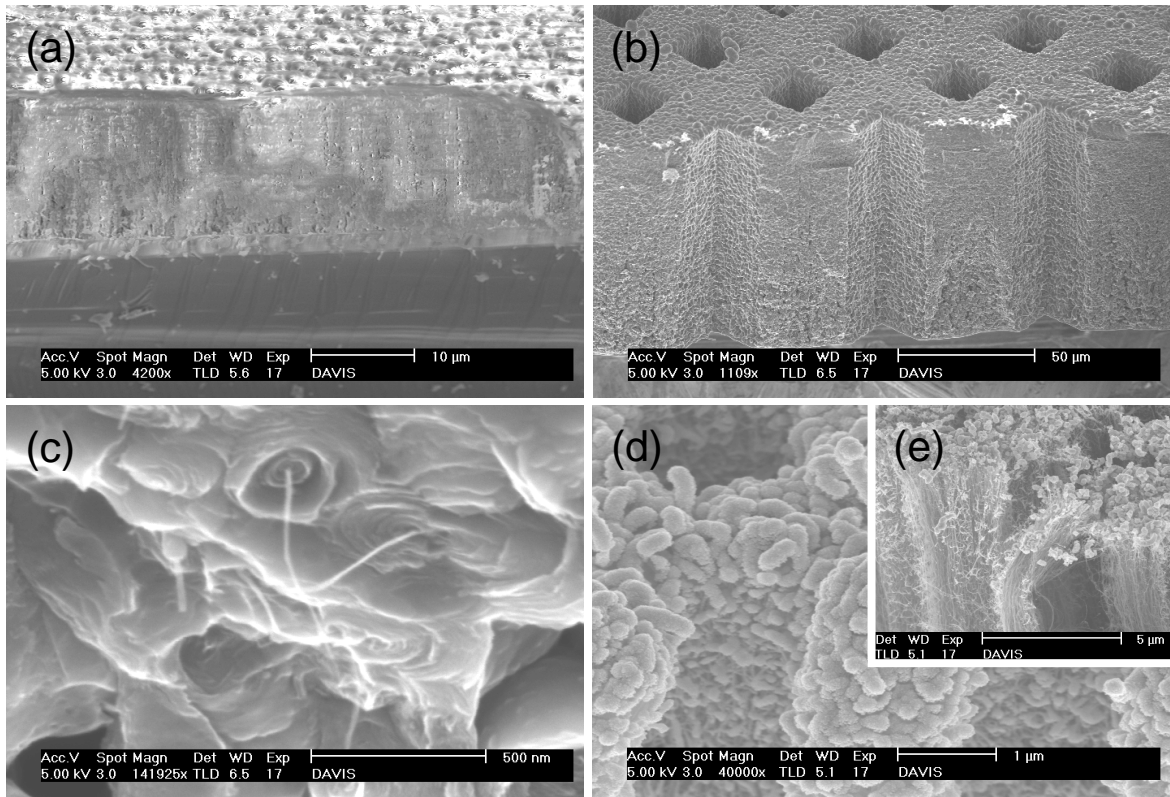
Figure 2.15 Results from filling with silicon nitride, amorphous carbon, and physical vapor deposition. **(a)** A silicon nitride-filled forest, cleaved and shown at 50° tilt. The nanotubes span the central 1/3 of the image, with tubes oriented vertically. **(b)** A patterned carbon nanotube forest filled in with amorphous carbon, broken open. **(c)** A higher magnification image of a broken edge of the carbon-filled forest in (b). **(d)** The top of a patterned forest coated only on the outside by evaporation of indium tin oxide. **(e)** The forest in (d) broken open to reveal uncoated tubes inside.

Physical vapor deposition techniques like evaporation and sputtering don't fill the forests but instead just coat the top and sides, which may be useful for certain applications. As an example, we evaporated indium tin oxide on a patterned forest.

2.6.3   Results

Results for the filling processes described in Sec. 2.6.2 are shown in Fig. 2.15.

2.7 Release

2.7.1 Methods

As discussed in Sec. 2.5.2, LPCVD coats the tubes with silicon, but also forms a "floor layer" of silicon in regions where there is no forest growth (also shown in Fig. 2.1(f)). This layer must first be removed to expose the underlying sacrificial layer so that parts of the structure may be released. We found that the easiest way to remove the floor layer is by a short O_2/CF_4 reactive ion etch (RIE), although a wet chemical etch might be made to work too (this would be a cheaper and more scalable alternative for industrial applications). For the RIE step, we used an Anelva RIE DEM-451, at 100 W, 100 mTorr, flowing 3.1 sccm of O_2 and 25 sccm of CF_4. We etched the floor layer for 5-9 minutes, depending on the size of the floor layer features we were trying to etch. In addition to removing the floor layer, this also removes a thin layer from the top of the coated nanotube structures. However, this is not a noticeable decrease in size for the MEMS devices since the devices are so tall compared to the thickness of the floor layer.

2.7.2 Results

The PECVD-deposited SiO_2 sacrificial layer, when etched with Buffered Oxide Etch (BOE, 1 HF : 5 NH_4HF : 5 H_2O) was found to etch at a rate of about 100 μm/h. Devices were put in BOE for as long as necessary to release the dynamic parts of the MEMS device (usually 20-30 minutes), while the larger parts of the device remain anchored to the substrate. Fig. 2.16 shows part of a MEMS device after release.
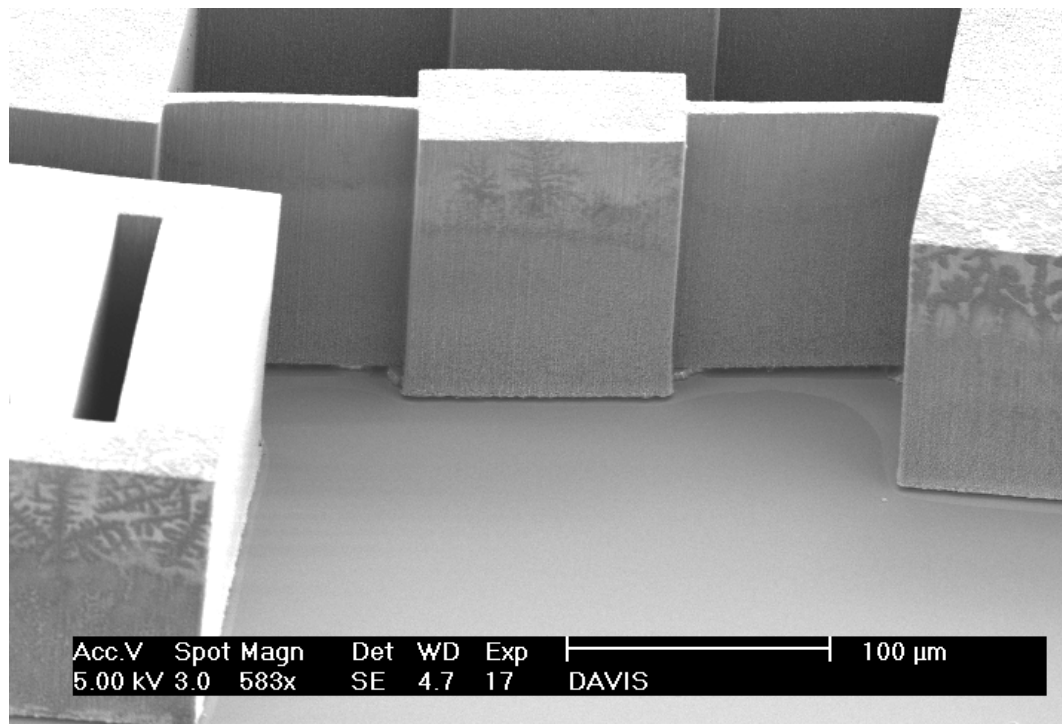
Figure 2.16 Part of a MEMS device after removal of the underlying 3 μm sacrificial SiO_2 layer. Large features such as the block on the right side of the image are not released, and act as anchor points for smaller, moving parts. The dendritic patterns on some parts of the device are probably dried salts from the Buffered Oxide Etch.

2.8 Resistivity

2.8.1 Methods

The resistivity of multi-walled carbon nanotubes can vary widely, around about 10^{-3} Ω cm to 10^1 Ω cm, depending on their atomic structure and the defects present [17]. They can exhibit ballistic conduction over distances of several micrometers at room temperature [18]. Undoped polycrystalline silicon, however, has a much higher resistivity: around 10^6 Ω cm, with little dependence on deposition conditions or crystal morphology [19]. The question naturally arises: does the nanotube framework embedded in polysilicon contibute significantly to its conductivity? If there is sufficient contact between nanotubes even after coating with silicon, we would expect that to be the case. This is an important question because the active parts of MEMS devices usually must be made from conductive materials, since they are often activated by, or perform some sensing function by, current or the accumulation of charge.

To test the resistivity of the coated nanotube material, squares of iron catalyst 0.5 cm on a side were fabricated and forests of various heights from 3 to 23 μm were grown. These forests were then filled, some with 300 nm of undoped polysilicon by LPCVD, some with silicon nitride, and some with 20 nm of silicon followed by about 150 nm of silicon nitride. The resistivity of those samples was found using a standard collinear four point probe measurement device (Magne-tron Instruments 750-1) with a probe spacing of 1.57 mm.

We expect to see a hyperbolic dependence of sheet resistance on the forest height, and a constant resistivity for various forest heights as suggested by the following argument:

If we define the conductance of a particular sample with a thickness t as $G(t) = 1/R(t)$, and assume that each infinitesimal thickness dt has the same conductivity

$dG = c_1 dt$, with c_1 a constant, then conductance is given by $G = \int dG = \int c_1 \, dt$, and the resistance measured across the sample will be

$$R_{meas} = \frac{1}{\int_0^t c_1 \, dt'} = \frac{c_2}{t} \tag{2.1}$$

and since the measured resistance will be proportional to the sheet resistance (which is the quantity we want) then

$$R_{sheet} = \frac{k}{t} \tag{2.2}$$

with k a constant.

To find this hyperbolic dependence, we measured sheet resistance by four-point probe as described previously in this section. Sheet resistance is measured in ohms per square (Ω/sq) and is a ratio of the voltage measured by two inner collinear probes due to the current passed between two outer collinear probes, multiplied by a geometry-dependent factor C. The value of C depends on the ratio of the probe spacing to the size of the sample and may be obtained from the method of images or may be looked up in tables such as those in an excellent paper by Smits [20]. In our case, $C = 2.458$.

$$R_{sheet} = \frac{V}{I} C \tag{2.3}$$

On an infinite sheet with thickness t, the four-point probe will introduce voltage gradients perpendicular to the surface. If t is approximately equal to or less than the spacing of the probes, these gradients are negligible and the slice can be treated as an infinitely thin slice.* In that case, the "body resistivity" (or just "resistivity"), ρ,

---

*We can also introduce a correction factor F to account for the assumption that there are no voltage gradients perpendicular to the surface. This means resistivity is given by

$$\rho = \frac{V}{I} C F t \tag{2.4}$$

Strictly speaking, the correct solution for the resistivity of a finite, thick sheet would require analysis using a three-dimensional method of images. However the value of F may be more simply calculated

is

$$\rho = R_{sheet}t \tag{2.5}$$

Therefore,

$$\rho = \frac{V}{I}Ct \tag{2.6}$$

Although this expression seems to depend on t, it is actually independent of t since the measured voltage V is also a function of t. It should give an approximately constant value for the resistivity of forests of various thicknesses when V, I, and t are measured.

2.8.2 Results

From 21 different samples prepared as described in the previous section, the sheet resistance was found to have a hyperbolic dependence on forest height (Fig. 2.17), and the resistivity of the composite was found to be about 4 Ω.cm, approximately constant and independent of both the filler material and the height of the forest. The measured resistivity is six orders of magnitude lower than the resistivity of undoped polysilicon and 14 orders of magnitude lower than that of silicon nitride. The vertically-oriented nanotubes seem to provide a horizontal conducting path through the composite material. The author has been unable to find values for the resistivity in the horizontal direction of a vertically-aligned nanotube forest but suspects there are probably significant resistances after filling with silicon at the junctions between tubes. The resistivity is about equal to the resistivity of crystalline silicon doped with

for a thick sample of infinite extent, and that value could serve as a first-order correction for a finite, thick sample. Since the forests measured were much shorter than the probe spacing, F is approximately 1. However, it is mentioned in this footnote since for much taller filled forests that may be measured in the future it may play a role. Furthermore, this derivation is for an isotropic material and vertically-aligned coated carbon nanotubes are highly anisotropic, so that may add an additional inconsistency more accurate future measurements.

Figure 2.17 Graph of sheet resistance and resistivity vs thickness of the composite. **(a)**) The sheet resistance of the coated forests vs. forest height. The graph follows the hyperbolic law predicted in the Methods section. **(b)** Resistivity of the coated forests vs. forest height. Although undoped polysilicon and silicon nitride have very different conductivities (typically about 8 orders of magnitude different), the resistivity of a silicon-filled forest and a nitride-filled forest appears to be about the same, and both composites have a resistivity of about 6 orders of magnitude lower than bulk undoped polysilicon.

P at 10^{15} cm^{-3}), which may be low enough for many MEMS devices. By filling with more conductive materials like metals, it may be possible to achieve lower resistivities by reducing the contact resistance at nanotube-nanotube junctions. Fig. 2.18 is a tilted SEM image showing the corner of one of the Si-filled forests used to measure resistivity.

This is significant because until now, MEMS have usually been made from heavily doped silicon since it is easy to micromachine and is electrically conductive. With the CNT framework technique, conductive MEMS may be made for the first time using
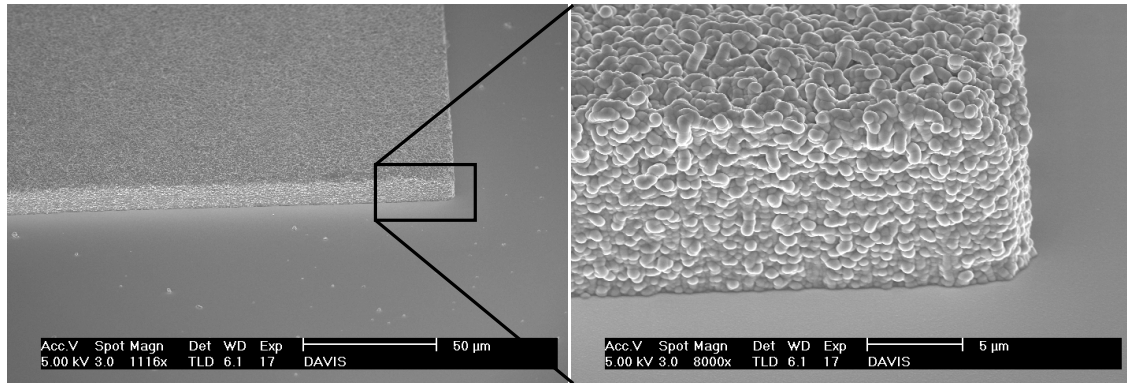
Figure 2.18 The corner of one of the polysilicon-filled forests that were used for four-point resistivity measurements. Image taken at 50° tilt.

insulating materials like silicon nitride.

2.9 MEMS Devices Fabricated

2.9.1 Introduction

This thesis is an attempt to present a new technique for making MEMS, not to design geometrically-better MEMS. As such, this section only presents several working MEMS briefly, without in-depth characterization or optimization. These devices are not new and they can be found, along with the relevant mathematical formulas, in many published articles or textbooks. Therefore they are only presented in closing as proof of the applicability of the present technique to the field of microelectromechanical systems. Further characterization of CNT-framework MEMS and comparison to the industry standard remains the work of future experimenters.

2.9.2 Bistable Mechanisms

Bistable mechanisms (BSMs) provide a way to store a state mechanically, analogous to a computer 'bit'—a 1 or a 0. They may be useful as micro-switches or micro-

valves requiring two well-defined positions [21], or as accelerometers since they can be designed to move from one position to another for a known force [22].

Two different geometries for BSMs were fabricated from both silicon-filled and nitride-filled forests. The two geometries for the silicon-filled BSMs are shown in Fig. 2.19 (a), and one of the geometries for the silicon nitride-filled BSMs is shown in Fig. 2.14 (although both geometries work for both fillers).

2.9.3 TIMs

Thermomechanical in-plane microactuators (TIMs) are linear motors that move a central shuttle piece when a current is passed through the narrow legs, due to thermal expansion of the legs. The legs are designed to be at a slight angle to the pads and the central shuttle piece. We made TIMs of two different sizes and observed displacement of up to 10 μm (Fig. 2.19 (b) and (c)).

Ordinary TIMs are usually made from heavily-doped polysilicon which has a lower resistivity than the nanotube composite. High voltages (above 100-150 V) were necessary to get noticeable movement of our devices, due to the relatively low resistivity of the nanotube composite (see Sec. 2.8). Some devices even exploded as higher voltages (up to 300 V) were applied. This problem seemed to disappear when constant current, rather than constant voltage was applied, but it may have also been sometimes due to the shuttle and legs being not properly released (since some devices that were clearly not properly released were some of the ones that exploded). However, we do not think that the high voltages needed for actuation of these devices represents a fundamental limitation of this technique, since the filler material may be selected from a wide range of materials. For example, the forest could be filled with heavily-doped silicon or something even more conductive (like a metal). It is therefore likely that the TIMs fabricated in this way will require even lower voltages for actuation and
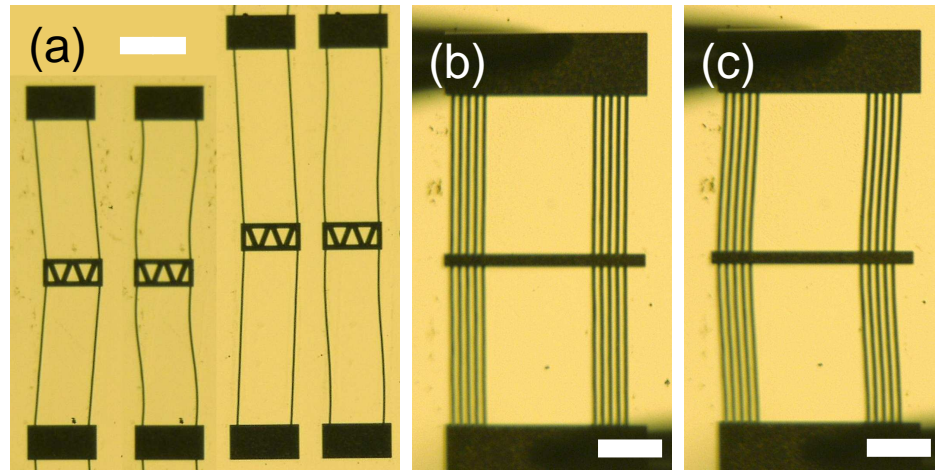
Figure 2.19 Composite optical microscope image of BSMs and TIMs made from silicon-filled CNT forests. **(a)** Two geometries for bistable mechanisms (BSMs), each shown in the two stable positions. Scale bar 200 μm. **(b)** A thermomechanical in-plane microactuator (TIM), shown in the 'off' state (no current flowing). Scale bar 100 μm. **(c)** The same TIM in the 'on' state. Scale bar 100 μm.

therefore have lower power consumption than the current state-of-the-art. It is also likely that MEMS designers may choose a filler material with high thermal expansion coefficient in order to further improve their devices.

2.9.4 Comb Drive

A comb drive is another kind of linear motor. Interdigitating teeth (one set fixed, one movable) attract or repel one another when electrically charged. Comb drives are often used as accurate micro-scale positioners. High aspect ratios are particulary important in comb drives and other capacitive MEMS since they reduce the effect of fringing fields and increase the capacitance of the device, thereby increasing the available force for a given voltage. High aspect ratios also help reduce out-of-plane motion. We made a silicon-filled comb drive as shown in Fig. 2.20.

The comb drive shown is only about 20 μm tall, giving the teeth an aspect ratio
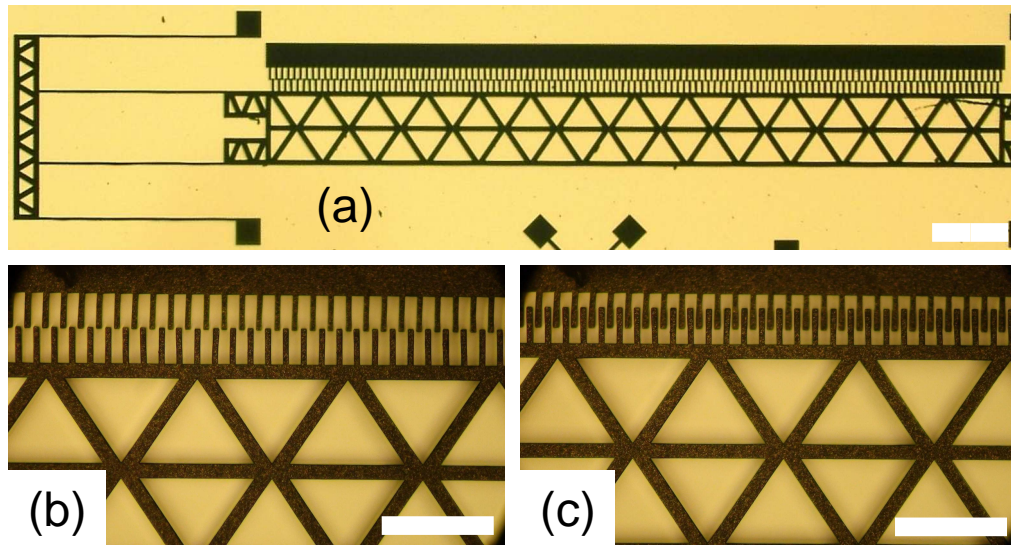
Figure 2.20 Si-CNT composite comb drive. **(a)** A comb drive, about 20 μm tall. The whole device would not fit in the field of view of the microscope, but the parts not shown are symmetric with the parts shown. Scale bar 300 μm. The comb drive teeth are shown disengaged (0 V) and engaged (160 V) in **(b)** and **(c)** respectively. Scale bars are both 150 μm.

of only about 3:1, but this may be improved in future devices. We made devices with higher aspect ratios but the long solid pad shown at the top of the comb drive in Fig. 2.20(a) tended to detach from the substrate during the release step because it was so wide and tall that it was not completely filled with silicon in the center. This meant that the pad was poorly adhered when the sacrificial oxide layer was etched far enough to release the moving part of the device. In future devices, the pad may be redesigned with vapor access holes (discussed in Sec. 2.5.2) that are small enough to allow the silane gas to enter and small enough so that the floor layer in the holes is not etched in the floor layer etch step, perhaps 1-3 μm in diameter. A comb drive that worked is shown in Fig. 2.20(b) and (c) with the teeth disengaged and engaged, respectively.

Chapter 3

Conclusions and Future Directions

We have made novel carbon nanotube composites by filling a low-density forest of carbon nanotubes with various materials by chemical vapor deposition and demonstrated several applications. These composites are particularly interesting for microfabrication of MEMS because

- Nanotube forests can be filled with a variety of materials. We have filled forests with undoped polysilicon, silicon nitride, and amorphous carbon, but it is likely that many other materials may be deposited as fillers.

  - By filling with a material that is resistant to harsh chemical environments (e.g. teflon) or high temperatures (e.g. tungsten), it may be possible to make MEMS sensors or actuators for previously impossible applications, such as measuring vibrations in turbine engines or geological drill heads.

  - The CNT framework technique may allow MEMS engineers to exploit the interesting properties (e.g. ferromagnetic, ferroelectric, piezoelectric, or other properties) of a variety of materials. These properties are already the functioning principle behind some MEMS devices, but the high aspect

ratios attainable and versatility of the nanotube framework technique may improve those devices or suggest new applications.

○ Using the framework technique, it is likely that MEMS engineers can tailor the mechanical properties of their device for their application by coating nanotube forests with combinations of fillers. We have yet to measure the mechanical properties of combinations of fillers but it is likely that for example, a forest that is first halfway-filled with silicon and then filled with silicon nitride may result in a composite that has mechanical properties (like Young's modulus) that are approximately halfway between the silicon-nanotube and the nitride-nanotube composites. If correct, this would make available a continuous range of material properties by selecting combinations of fillers.

• The filler material only has to fill the interstices between tubes, so a relatively quick deposition (the equivalent of 300 nm or less on a planar substrate) can fill very tall forests tens or hundreds of micrometers tall (especially if they are designed with vapor access holes).

○ Since only 300 nm of deposition is required to form much larger structures this technique may reduce the amount of reactant gases needed, which is particularly important if the gas is expensive (such as copper ethylacetoacetate for CVD copper deposition [23]).

○ This process may even allow materials that have very slow CVD deposition rates to be used as fillers.

• The nanotubes provide an electrically conductive path through the composite.

○ Interestingly, forests filled with undoped polysilicon and forests filled with

silicon nitride both have about the same resistivity even though the two fillers have very different resistivities. This suggests that other insulators used as fillers may also result in an electrically conductive composite, possibly with similar resistivities to these silicon and nitride composites.

○ Until now it has been impossible to make conductive MEMS from insulators like silicon nitride, even if the insulator's mechanical properties were desirable. This may represent a route to more versatile design of conductive MEMS.

• The nanotube framework technique can result in high aspect ratio structures.

○ These high aspect ratio structures help keep the motion of devices in-plane, and allow capacitive MEMS like comb drives to have higher capacitances and less significant fringing fields.

○ These high aspect ratio structures have vertical sidewalls for the range of forest heights we have tried. There is no taper in the sidewalls. It is difficult to minimize sidewall taper in a DRIE process.

• Crossbars (or other self-supporting architectures) may be used to reliably grow thin forest walls taller than achievable without crossbars. We believe this is the first time this effect has been presented. Self-supporting architectures may prove to be crucial to MEMS design to maintain the compliance of small members while still growing tall structures.

• In order to take advantage of the high ultimate strength of individual nanotubes, it may be interesting in the future to have the filled nanotube forest aligned horizontally, parallel to the flexing members, rather than vertically, perpendicular to the flexing members. Horizontally-aligned nanotubes have been sucessfully

grown by Wei *et al.* [24]. The nanotubes could be grown in horizontally-aligned arrays, filled with a filler like silicon, polished on top by chemical-mechanical polishing, and then MEMS could be patterned using traditional etching techniques on the resulting substrate, aligning the flexing members parallel to the nanotube direction.

- This process only uses well-known techniques (evaporation, CVD, and etching) and equipment that is commonly found in a fabrication facility, and therefore may be highly integrable into current technologies.

- The simplicity, scalability, and cost-effectiveness have not yet been fully investigated but seem promising and competitive with the current state-of-the-art.

Bibliography

[1] I. Gunjishima, T. Inoue, S. Yamamuro, K. Sumiyama, and A. Okamoto, "Growth of vertically aligned carbon nanotubes from highly active Fe-Ti-O nanoparticles prepared by liquid-phase synthesis," Japan. J. App. Phys. **46,** 3700–3703 (2007).

[2] A. J. Hart and A. H. Slocum, "Rapid growth and flow-mediated nucleation of millimeter-scale aligned carbon nanotube structures from a thin-film catalyst," Phys. Rev. Lett. **110,** 8250–8257 (2006).

[3] M. S. Dresselhaus, G. Dresselhaus, and P. Avouris, *Carbon Nanotubes: Synthesis, Structure, Properties, and Applications* (Springer-Verlag, New York, 2001).

[4] A. M. Cassell, J. A. Raymakers, J. Kong, and H. J. Dai, "Large scale CVD synthesis of single-walled carbon nanotubes," J. Phys. Chem. B **103,** 6484–6492 (1999).

[5] D. Kim, S. H. Lim, A. J. Guilley, C. S. Cojocaru, J. E. Boure, L. Vila, J. H. Ryu, K. C. Park, and J. Jang, "Growth of vertically aligned arrays of carbon nanotubes for high field emission," Thin Solid Films **516,** 706–709 (2008).

[6] S. Fan, M. G. Chapline, N. R. Franklin, T. W. Tombler, A. M. Cassell, and H. Dai, "Self-oriented regular arrays of carbon nanotubes and their field emission properties," Science **283,** 512–514 (1999).

[7] J. N. Barisci, G. G. Wallace, D. R. MacFarlane, and R. H. Baughman, "Investigation of ionic liquids as electrolytes for carbon nanotube electrodes," Electrochem. Comm. **6,** 22–27 (2004).

[8] M. Tanaka, "An industrial and applied review of new previous MEMS devices features," Proc. 32nd Int. Conf. on Micro- and Nano-Engineering **5–8,** 1341–1344 (2007).

[9] J. E. Jang, S. N. Cha, Y. Choi, G. A. Amaratunga, D. J. Kang, D. G. Hasko, J. E. Jung, and J. M. Kim, "Nanoelectromechanical switches with vertically aligned carbon nanotubes," Appl. Phys. Lett. **87,** 163114 (2005).

[10] Y. Hayamizu, T. Yamada, K. Mizuno, R. C. Davis, D. N. Futaba, M. Yumura, and K. Hata, "Integrated three-dimensional microelectromechanical devices from processable carbon nanotube wafers," Nature Nanotechnol. **3,** 289–294 (2008).

[11] J. E. Jang, S. N. Cha, Y. J. Choi, J. Young, D. J. Kang, T. P. Butler, D. G. Hasko, J. E. Jung, J. M. Kim, and G. A. J. Amaratunga, "Nanoscale memory cell based on a nanoelectromechanical switched capacitor," Nature Nanotechnol. **3,** 26–30 (2008).

[12] L. Qu and L. Dai, "Direct growth of three-dimensional multicomponent micropatterns of vertically aligned single-walled carbon nanotubes interposed with their multi-walled counterparts on Al-activated iron substrates," J. Mater. Chem. **17,** 3401–3405 (2007).

[13] Lawrence Livermore National Laboratory, "Aerogels Terms," https://ipo.llnl.gov/technology/profile/aerogel/Terms/index.php (Accessed March 7, 2008).

[14] *Chemical Vapor Deposition*, J. H. Park and T. S. Sudarshan, eds., (ASM International, Materials Park, OH, 2001).

[15] J. K. Bhardwaj and H. Ashraf, "Advanced Silicon Etching Using High-density Plasmas," Proc. SPIE **2639,** 224–233 (1995).

[16] M. F. Aimi, M. P. Rao, N. C. MacDonald, A. S. Zuruzi, and D. P. Bothman, "High-aspect-ratio bulk micromachining of titanium," Nature Mat. **3,** 103–105 (2004).

[17] J. Gaillard, M. Skove, and A. M. Rao, "Mechanical properties of chemical vapor deposition-grown multiwalled carbon nanotubes," Appl. Phys. Lett. **86,** 233109–233111 (2005).

[18] C. Berger., Y. Yi, Z. L. Wang, and W. A. de Heer, "Multiwalled carbon nanotubes are ballistic conductors at room temperature," Appl. Phys. A **74,** 363–365 (2002).

[19] T. I. Kamins, *Polycrystalline Silicon for Integrated Circuits and Displays* (Kluwer Academic Publishers, Norwell, MA, 1998).

[20] F. M. Smits, "Measurements of Sheet Resistivities with the Four-Point Probe," Bell System Tech. J. pp. 711–718 (1958).

[21] B. D. Jensen and L. L. Howell, "Bistable configurations of compliant mechanisms modeled using four links and translational joints," Journal of Mechanical Design **126,** 657–666 (2004).

[22] J. W. Wittwer, M. S. Baker, D. D. Epp, and J. A. Mitchell, "MEMS Passive Latching Mechanical Shock Sensor," In *2008 Proceedings of the ASME International Design Engineering Technical Conferences and Computers and Information in Engineering Conference, DETC2008*, (2008).

BIBLIOGRAPHY45

[23] A. Devi and S. A. Shivashankar, "Thermal chemical vapour deposition of copper films from copper ethylacetoacetate: microstructure and electrical resistivity," J. Mater. Sci. Lett. **17,** 367–369 (1998).

[24] B. Q. Wei, R. Vajtai, Y. Jung, J. Ward, R. Zhang, G. Ramanath, and P. M. Ajayan, "Assembly of Highly Organized Carbon Nanotube Architectures by Chemical Vapor Deposition," Chem. Mater. **15,** 1598–1606 (2003).